Automatic Detection of Algal Blooms Using Sentinel-2 MSI and Landsat OLI Images

Dandan Xu, Yihan Pu, Mengyuan Zhu, Zhaoqing Luan, and Kun Shi

***Abstract*—Algal bloom is a serious global issue for inland waters, posing poses a serious threat to aquatic ecosystems. The timely and accurate detection of algal blooms is critical for their control, management and forecasting. Optical satellite imagery with short revisit times has been widely used to monitor algal blooms in marine and large inland waters. However, such images typically are of coarse resolution, limiting their utility to map algal blooms in small inland waters. We developed a new method to map the spatial extent of algal blooms using sentinel-2 multispectral instrument (MSI) and Landsat operational land imager (OLI) images with higher spatial resolution but lower temporal resolution based on the concept of local indicator of spatial association. The mapping results was applied to measure the duration and frequency of algal blooms in Lake Taihu from 2017 to 2020. Our results show that the developed methodology is able to extract the spatial distribution of moderate algal blooms using near-infrared and red-edge bands (bands 6, 7, 8, and 8a of sentinel-2 MSI images or band 5 of Landsat OLI images) by comparison with MODIS FAI data ($R2 = 0.888$ for sentinel-2 MSI and $R2 = 0.85$ for Landsat OLI, $P < 0.05$). However, the temporal resolution of combined Landsat OLI and sentinel-2 MSI images (i.e., up to 2–3 days) is insufficient to monitor algal blooms during the summer time in Lake Taihu due to cloud effects and rapid algal change. Our research has benefits for the management of small inland waters with complex water conditions.**

***Index Terms*—Algal bloom, cyanobacteria, spatial autocorrelation, sentinel-2 multispectral instrument (MSI), Landsat operational land imager (OLI).**

Manuscript received July 15, 2021; revised August 8, 2021; accepted August 15, 2021. Date of publication August 18, 2021; date of current version September 7, 2021. This work was supported by the Jiangsu Agricultural Science and Technology Independent Innovation Fund under Grant CX (18) 2026, in part by the National Natural Science Foundation of China under Grant 41922005, in part by the Six Talent Peaks Project in Jiangsu Province under Grant TD-XYDXX-006, in part by the Natural Science Foundation of Jiangsu Province under Grant BK20180769, in part by the Scientific Instrument Developing Project of the Chinese Academy of Science under Grant YJKYYQ20200071, and in part by the NIGLAS foundation under Grant E1SL002. *(Corresponding author: Kun Shi.)*

Dandan Xu and Yihan Pu are with the Department of Ecology, College of Biology and the Environment, Nanjing Forestry University, Nanjing 210037, China (e-mail: dandan.xu@njfu.edu.cn; pyh1997@njfu.edu.cn).

Mengyuan Zhu and Kun Shi are with the State Key Laboratory of Lake Science and Environment, Nanjing Institute of Geography and Limnology,Chinese Academy of Sciences, Nanjing 210008, China (e-mail: myzhu@niglas.ac.cn; kshi@niglas.ac.cn).

Zhaoqing Luan is with the Co-Innovation Center for Sustainable Forestry in Southern China, Nanjing Forestry University, Nanjing 210037, China (e-mail: luanzhaoqing@njfu.edu.cn).

This article has supplementary downloadable material available at https://doi.org/10.1109/JSTARS.2021.3105746, provided by the authors.

Digital Object Identifier 10.1109/JSTARS.2021.3105746

I. Introduction

INLAND waters, including rivers and lakes, provide various ecosystem services, regulate microclimate, maintain biodiversity, and supply habitat for flora and fauna [1]. They are closely tied to human populations as water supplies for drinking, aquaculture, industry and tourism [2], [3]. However, around the world, algal blooms of high intensity and duration in inland waters are being frequently reported [4]–[6]. The causes for this phenomenon include nutrient enrichment from agricultural, industrial and urban runoff [7], [8], hydrological alteration from dam construction [4], and climate change [1], [6]. Algal blooms disrupt ecological equilibrium and food webs [1], [3], [7], [9]–[11], and threaten freshwater systems for drinking, irrigation, fishing and recreation [2], [12]–[14].

It is increasingly beneficial to detect algal blooms accurately and timely to control, manage, and forecast them in inland waters [15], [16]. Algal blooms are generally characterized by very complex temporal variability due to their capacity to replicate quickly and migrate vertically within the water column [3,] [11], [12]. Field monitoring with few observations, including conventional ship and station-based investigations, are unable to adequately sample the occurrence, frequency, spatial extent and magnitude of algal blooms in inland waters [1], [5], [12], [14], [17], 18]. However, satellite imagery with diverse spatial and temporal resolutions has great potential for timely and accurate algal bloom monitoring at large spatial extents, frequency, drifting rates and occurrence duration [6], [19], [20].

Landsat series, moderate resolution imaging spectroradiometer (MODIS) and medium resolution imaging spectrometer (MERIS) are the most commonly used satellite products for monitoring the spatial extents and temporal dynamics of algal blooms in inland waters [1], [6]. Previous studies have demonstrated the frequent mapping capacity of MODIS and MERIS products in both marine and large inland waters globally, due to their high temporal resolution (often with 1–3 days revisits) [12], [15], [17], [21]–[29]. However, their spatial resolution is too coarse for algae monitoring for small inland waters. Landsat series, with a much higher spatial resolution (30 m) and longest earth observation records (since the 1980s), ensure the long-term algae monitoring in inland waters, especially small water bodies [6], [30], [31]. However, Landsat's utility for mapping the temporal variability of algal blooms is seriously limited by the long revisit intervals (16 days) [1]. Other imagery with high spatial resolution explored by previous studies, including RapidEye, HJ-1, SPOT-4/5, SPOT-6/7, and Worldview-2 [2],

[4], [30], [32]–[36], are restricted by their cost for continuous monitoring of algal blooms [23]. Among all, the two latest generation of multispectral sensors on board of Landsat 8 and sentinel-2 are both promising for detailed water quality and constituent analysis in inland waters due to their fine spatial resolution (10–30 m), improved spectral configuration in visible and near-infrared (NIR) wavelength regions, and high radiometric sensitivity [3], [6], [14], [30], [31], [33], [37]–[39]. A few studies have demonstrated the good performance of sentinel-2 multispectral instrument (MSI) or Landsat operational land imager (OLI) images for monitoring algal blooms in inland waters [35]–[37], [39]. Moreover, the combination of sentinel-2 MSI and Landsat OLI would generate images with high frequency of overpass (up to every 2–3 days), improved spectral band configuration, and fine spatial resolution (10–30 m) with global availability [37], which meets the essential criteria for continuous monitoring of algal blooms [23]. Therefore, it is worth testing whether the combination of sentinel-2 MSI and Landsat OLI images have the potential to extract the frequency and duration of algal bloom outbreaks in inland waters.

Methods applied for algal bloom extraction from sentinel-2 MSI, Landsat OLI and other optical images with high spatial resolution are often based on a given threshold of estimated Chlorophyll-a (Chl*a*) or various spectral indices [e.g., floating algae index (FAI), normalized difference chlorophyll index, maximum chlorophyll index (MCI), NIR to red ratio] [13], [14], [30], [34], [40], [41], which were originally applied to ocean color data [4], [18], [20], [23], [24], [35], [42]–[46]. However, the applications of such methods are often limited to the specific spectral band configurations and affected by complex water conditions of inland waters [turbidity, shallow depth, high concentrations of color dissolved organic matter (CDOM) and total suspended matter (TSM)] [13]. The algorithms for Chl*a* estimation and most indices require visible bands due to the absorption characteristics of Chl*a* [18], [47]. However, turbid waters have similar spectral signals as cyanobacterial scums in red and green bands [10], [48], which challenges the discrimination of algal bloom in different water conditions regarding to the degree of turbidity. Therefore, such threshold methods sometimes tend to give a false positive detection of algal blooms [47], [49], [50]. Due to the complexity of inland waters, previous studies need to adjust the thresholds of Chl*a* or spectral indices for different locations based on published studies, experience, visual identification of algal bloom pixels and field sampling [6], [14], [38]; these approaches lack the capacity to be applied to other locations and often need to be calibrated to ensure cross-sensor and temporal consistency [30], [38]. Therefore, it is important to develop a new method for algal bloom mapping to maintain temporal consistency and avoid illogical classification results.

Reflectance-classification methods can be sufficient for mapping algal blooms with the spectral bands located in visible and NIR wavelength regions [47]. Few research applied classification algorithm (artificial neural network [2]) to estimating algal scums with such bands. Spectral bands in red-edge and NIR regions show much better results for the discrimination of algal blooms in inland waters than visible bands (e.g., red-edge band used for MCI algorithm [23] and NIR band used for FAI algorithm [51]), which are robust to detect high-conentration algal blooms under the influence of turbidity, CDOM and TSM. High-conentration algal blooms form scums, patches, thin films or thick mats on the water surface [i.e., severity levels by visual cyanobacteria index (VCI)] [52], which were presented as surface clusters in inland waters. Classification methods integrating spatial autocorrelation have high potential to capture such algal blooms characterized by surface clusters to avoid illogical results using threshold methods. The local indicators of spatial association (LISA) is a method for capturing spatial clusters with the potential to extract relatively homogeneous land cover types for environmental and ecological research [53]. Several studies have indicated that it could improve temporal consistency and accuracy of land cover classification while preserving spatial consistency [54]. Zhang *et al.* successfully monitored river plume in Lake Taihu using LISA [55]. High-concentration algal blooms have similar spectral characteristics as land vegetation in red-edge and NIR wavelength regions [1], resulting distinct higher reflectance than turbid water [40], [56]. However, it is not explored whether NIR band and red-edge bands have different performance in classifying high-concentrated algal blooms. For these reasons, it is worth exploring the potential of classification algorithms based on the concept of LISA to extract the spatial extent of algal blooms with different spectral bands in the wavelength regions of red-edge and NIR.

Therefore, this article aims to test the potential of LISA with sentinel-2 MSI and Landsat OLI imagery to monitor the spatial extent, frequency and occurrence duration of algal blooms in inland lakes. The specific objectives are: to develop an automatic method for mapping algal blooms with batch processing capacity based on the LISA concept; to evaluate the performance of different spectral bands for mapping algal blooms, and to investigate the occurrence frequency and duration of algal blooms by combing the mapping results from sentinel-2 MSI and Landsat OLI images.

II. Materials and Methods

A. Study Area

Lake Taihu is the third-largest freshwater lake in China, with 2338 km^2 of open water and a water storage volume of 4.4×10^9 m^3 (see Fig. 1) [57]–[60]. It is a shallow inland eutrophic lake with a maximum depth of 2.6 m and average depth of 1.9 m [57]–[60]. It is a drinking water source for more than 40 million people and plays an important role in aquaculture, tourism and flood control [8], [58], [59]. However, the large population, urbanization, industrial development, intensive agriculture and tourism activities caused hypereutrophic and experienced algal blooms in Lake Taihu since 1990s [61]–[63]. During the past 20 years, more than 25% area of the whole lake has been frequently covered by floating algae in spring and summer due to eutrophication [62]–[65]. A very severe cyanobacterial bloom occurred in May 2007, depriving more than 2 million people from drinking water for 8 days (May 30th to June 6th) [60]. This event attracted the government's attention, and the Jiangsu hydrology and water resources investigation

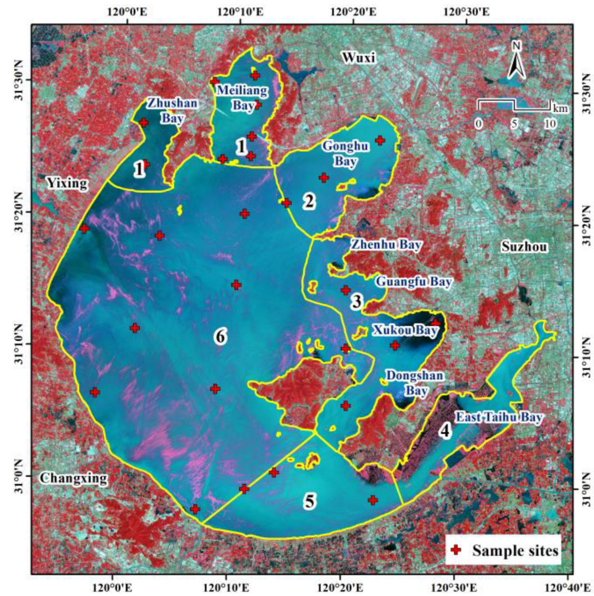

Fig. 1. Sample sites in the study area (Lake Taihu, China). The background image is from sentinel-2 MSI acquired on August 17, 2019, composed of near-infrared, red, green bands in red, green, and blue color tons. The pink color within the lake area shows algal bloom outbreaks.

bureau have been conducting daily inspections of algal bloom area from April to October every year since 2009 [59].

Lake Taihu is divided into six management sections (see Fig. 1). Depending on the lake's hydrodynamics and intensity of human activities, cyanobacteria blooms occurred mainly in section 1 (Meiliang and Zhushan Bays), section 2 (Gonghu Bay), and section 6 (see Fig. 1) [48], [59], [66], [67]. Section 3, including Zhenhu, Guangfu, Xukou, and Dongshan Bays (see Fig. 1), is typically dominated by macrophytes with three types of aquatic vegetation, including emergent (*Phragmites communis* and *Zizania latifolia*), submerged vegetation (*Elodea nuttallii*, *Potamogeton crispus*, *Myriophyllum spicatum*, *Potamogeton maackianus*, *Ceratophyllum demersum,* and *Vallisneria spiralis*) and floating-leaved vegetation (*Eichhornia crassipes*, *Lemna minor*, *Nymphoides peltata*, and *Trapa bicornis*) [57]. Section 4 (East-Taihu Bay) is a submerged vegetation region with good water quality and a productive fishery. Section 5 was originally dominated by floating-leaved vegetation [66], but now affected by algal blooms as well due to wind effects and the algal blooms from section 6 [60]. Therefore, researches also integrate sections 5 and 6 together and interpret it as northwest lake, central lake and southwest lake [13], [57], [58].

Lake Taihu was selected for this article due to the high frequency of algal bloom outbreaks, despite not being a small inland water body; a condition ideal for testing our method. Nevertheless, its frequency of algal outbreaks and size are both suitable to compare mapping results from sentinel-2 MSI and Landsat OLI images with MODIS FAI data.

B. Remotely Sensed Images

A total of 34 sentinel-2 MSI and 11 Landsat OLI images of high quality from 2017 to 2020 were downloaded from the United States Geological Survey (USGS) website[1] for this study (see supplementary material A for image acquiring dates). Landsat OLI images were already geometrically and atmospherically corrected (i.e., level 2 product). Sentinel-2 MSI images were previously geometrically corrected (i.e., level 1 product) when downloaded. The spatial resolutions of the sentinel-2 MSI images are 10, 20, and 60 m (i.e., the bands used for algal bloom mapping are near-infrared bands and red-edge bands with spatial resolution of 10 m and 20 m) and the spatial resolution of Landsat OLI image is 30 m. All the sentinel-2 MSI images were then radiometrically and atmospherically corrected via Sen2cor toolbox from SNAP software provided by European Space Agency, and resampled to a spatial resolution of 20 m using bilinear interpolation [68]. All the images were projected at universal transverse mercator Zone 51N, WGS1984. Thirty cloud-free MODIS images (see supplementary material A for the image acquiring dates) were used to calculate FAI to validate the mapping results from sentinel-2 MSI and Landsat OLI images.

C. Methodology

After preprocessed sentinel-2 MSI bands (i.e., NIR, SWIR1, and red-edge bands) and Landsat bands (i.e., NIR and SWIR1), LISA were conducted on all single bands to identify the significant, high value clusters, integrate the extraction results among bands and interpret the severity level of algal blooms (see Fig. 2). All steps were coded in a Python script (see supplementary materials) following a detailed workflow (see Fig. 2).

1) Preprocessing of sentinel-2 MSI/Landsat OLI Single Bands: Pre-processing steps included clipping the bands to the study area, raster conversion to NumPy array in python script and standardization of the NumPy array for both sentinle-2 and Landsat OLI

$$P = \frac{\sum (\rho - \bar{\rho})^2}{\mathrm{std}\,(\rho)} \tag{1}$$

where P is the standardized reflectance of each pixel; ρ is reflectance of each pixel for a single band; $\bar{\rho}$ and $\mathrm{std}(\rho)$ are the average reflectance and standard deviation of all pixels for the single band.

Red-edge, NIR and SWIR1 bands were selected for mapping algal blooms in this article for three reasons. First, turbid water has a strong influence on mapping algal blooms using spectral bands within the visible range (see Fig. 3; spectra downloaded from the USGS spectra library). Second shortwave infrared (SWIR2) band was not selected as it has been shown previously in Lake Taihu, it cannot distinguish algal blooms and open water [69]. Finally, algal blooms have higher reflectance in red-edge, NIR, and SWIR1 bands than turbid and open water (see Fig. 3).

2) Spatial Autocorrelation Analysis: Following all preprocessing steps, spatial autocorrelation was performed for each standardized NumPy array. During the spatial autocorrelation analysis, eight adjacent pixels (P_j) were selected as spatial neighbors for the pixel P_i (see Fig. 2) to calculate spatial autocorrelation index I_i [(2); built using to the concept of Local

[1][Online]. Available: https://earthexplorer.usgs.gov/

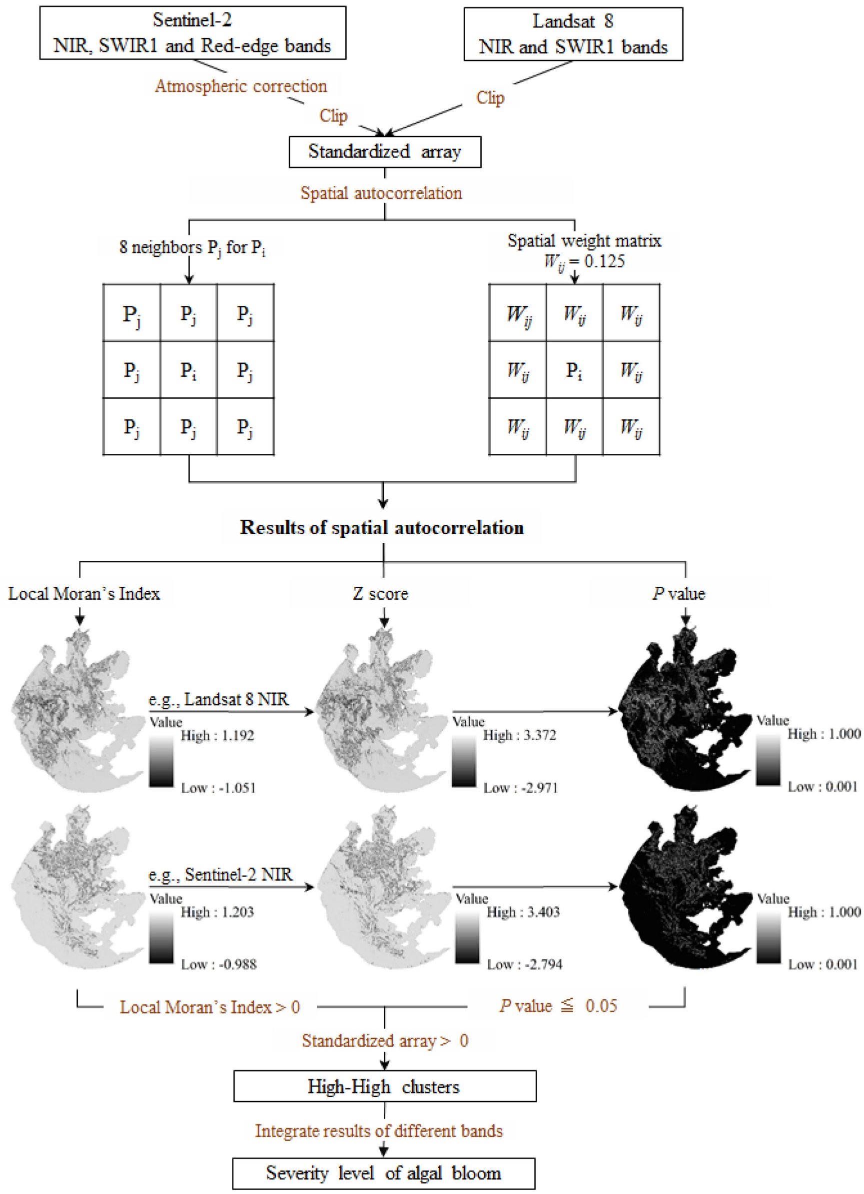

Fig. 2. Methodology flowchart (NIR: Near-infrared band; SWIR1: first shortwave infrared band; Red-edge bands of sentinel-2 MSI images: bands 5, 6, 7, and 8a).

Moran's Index] with spatial weight (W_{ij}) 0.125 for each neighbor (i.e., equal weight for eight neighbor pixels with the total weight for the spatial lag variable of 1) (see Fig. 2)

$$I_i = \frac{(n-1)\, P_i \sum_j W_{ij} P_j}{\sum_j P_j^2 + P_i^2} \tag{2}$$

where P_i is the standardized reflectance of one pixel on a single band (see Fig. 2), P_j is one of the eight spatial neighbors of P_i (see Fig. 2), W_{ij} is the spatial weight (see Fig. 2), and n is the number of spatial neighbours (8). I_i is the Local Moran's index that refers to the spatial association between a given pixel (P_i) and its spatial lag variable ($\sum_j W_{ij} P_j$) which was calculated using the spatial neighbors and their corresponding spatial weight.

Z score is the value of standard normal distribution, which is the test statistic for the significant test of Local Moran's index, I_i [i.e., spatial autocorrelation index, (3)].

P value was calculated using the corresponding test statistic Z for the analysis of Local Moran's Index using the python package "scipy.stats" [command line *st.norm.sf(abs(Z))*×*2*]. The High-High clusters were high values significantly clustered spatially in a single spectral band [i.e., the first "High" means P_i is significantly high on the standardized array; the second "high" means the value of its spatial lag variable ($\sum_j W_{ij} P_j$) was significantly high as well]. The high-high clusters were selected from the results of spatial autocorrelation according to three criteria (see Fig. 2): $I_i > 0$ (i.e., either high values or low values are clustered together), or the value in the standardized array is larger than zero (i.e., separate the high values clusters from

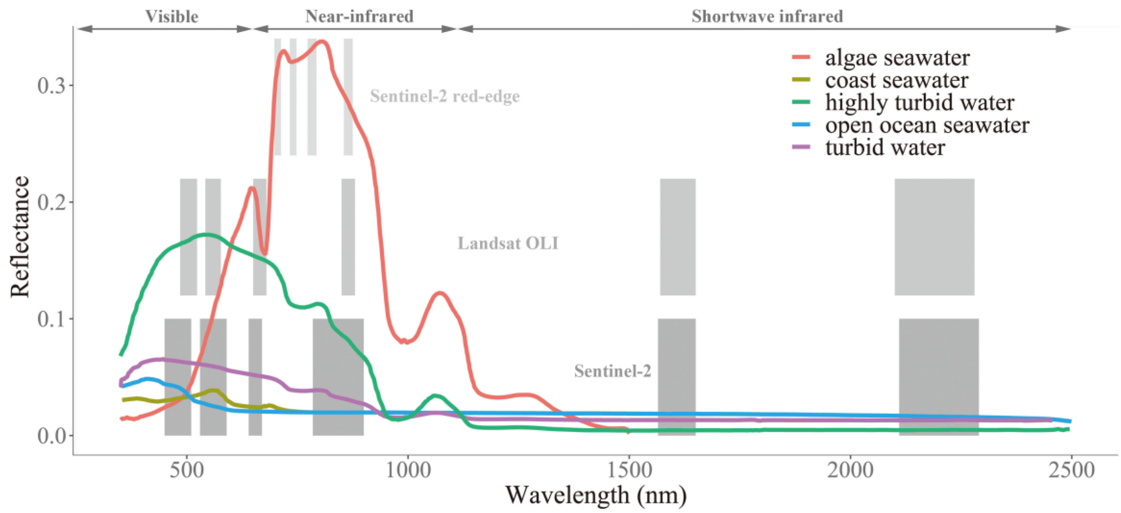

Fig. 3. Spectral characteristics of water in different conditions (spectra downloaded from USGS spectral library version 7[2] algal blooms (measured in Arkansas River, Leadville, Colorado, USA); coastal seawater (surface Chl*a* of 7.609 ug·L^{-1}); open ocean (surface mean Chl*a* of 2.97 ug·L^{-1}); turbid water (water mixed with montmorillonite of 0.50 g·L^{-1}); and highly turbid water (water mixed with montmorillonite of 1.67 g·L^{-1}).

low value clusters) for each band; or P value ≤ 0.05 (i.e., select statistically significant high value clusters out) where Z is the test statistic from standard normal distribution, I_i is the spatial autocorrelation index from (2), N is the total number of pixels for a single band, W_{ij} is the spatial weight for each neighbor, P is the standardized reflectance from (1), $\bar{P}$ is the average value of the standardized array calculated by (1).

3) Severity, Frequency, and Duration of Algal Blooms: After the high-high clusters were extracted from each band, the extracted area and spatial extent were compared among NIR, red-edge, and SWIR bands of sentinel-2 MSI and Landsat OLI images separately. The severity levels of algal blooms were determined based on area and spatial extent extracted from NIR, red-edge, and SWIR bands. The extracted area of algal blooms from those bands of both satellite images were validated using the FAI data calculated from MODIS images with the spatial resolution of 250 m (i.e., paired up MODIS images with sentinel-2 MSI or Landsat OLI image based the criteria of the same acquiring date) [70]. After mapping the severity of algal blooms, the mean values of the surface reflectance of moderate and severe algal blooms from all the spectral bands of Landsat OLI and sentinel-2 MSI images were calculated. These mean reflectance values were used to form the spectral profiles of both Landsat OLI and sentine-2 images for moderate and severe algal blooms.

To analyze the frequency and duration of algal blooms, high temporal resolution remote images are required. However, only 34 sentinel-2 MSI images and 11 Landsat OLI images with limited cloud cover were available for mapping. Therefore, we visualized 93 sentinel-2 MSI and 32 Landsat OLI images during 2017–2020 (i.e., all images acquired by both satellites including those with clouds) to collect a time series dataset with algal bloom occurrence information. The extracted algal bloom areas from the 34 sentinel-2 MSI images and 11 Landsat OLI images were added into the time series dataset, while zero areas of algal blooms were added to the dataset on dates when algal blooms were not observed in the images. For images with high cloud cover with known (observed) algal blooms, the area of algal blooms was recorded as missing in the time series dataset. The interpolation method (*na.approx*) in the "zoo" package of *R* software was used to fill missing data. The frequency, occurrence period and duration of algal blooms were then analyzed based on the time series dataset from 2017 to 2020.

4) Validation by *In Situ* Measured Chl*a* Data: *In situ* measured Chl*a* data in Lake Taihu were used to validate the frequency, occurrence period and duration of algal bloom outbreaks extracted from both sentinel-2 MSI and Landsat OLI images. *In situ* data were collected at all 32 sites in Lake Taihu (see Fig. 1) during February, May, August, and November, and s collected at 14 sites (including eight sites in sections 1 and 3 sites in sections 2 and 3 sites in the northern part of section 6; Fig. 1) for the other months during 2017–2019. Chl*a* pigments were extracted using 90% ethanol at 80 °C from the collected water samples. Chl*a* concentrations were calculated from the absorption coefficients at 665 and 750 nm.

[2]https://crustal.usgs.gov/speclab/QueryAll07a.php

$$\mathrm{Z} = \frac{I_i - \left(-\frac{1}{N-1}\right)}{\sqrt{\frac{8\times W_{ij}^2 \times \left(N - \frac{\sum (P-\bar{P})^4}{\left(\sum (P-\bar{P})^2\right)^2}\right)}{N-1} - \frac{27\times W_{ij}^2 \times \left(2\times \left(\frac{\sum (P-\bar{P})^4}{\left(\sum (P-\bar{P})^2\right)^2}\right) - N\right)}{(N-1)\times(N-2)} - \left(\frac{1}{N-1}\right)^2}} \tag{3}$$

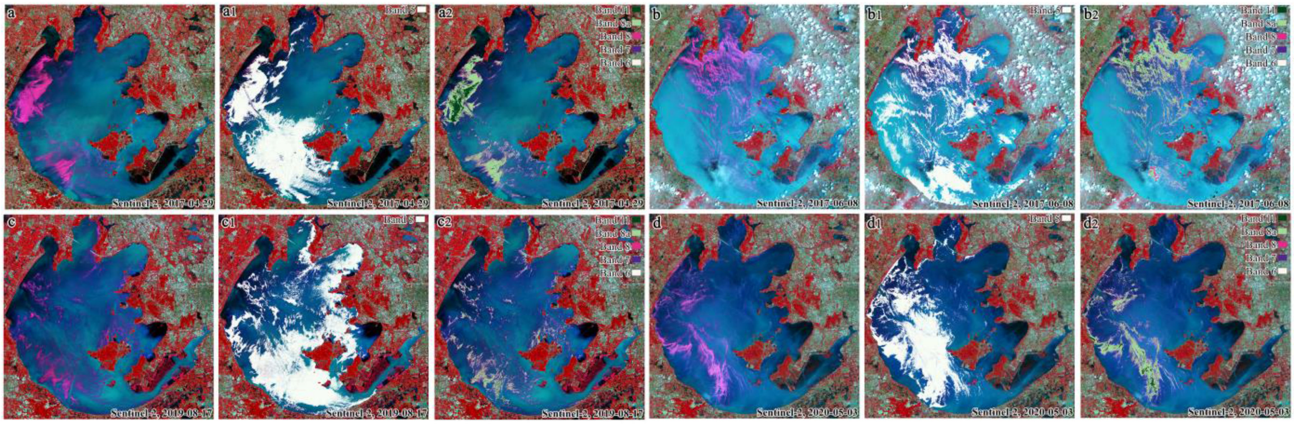

Fig. 4. Sample algal bloom extraction results from sentinel-2 MSI images. (a) Extractions from band 5 (a1), and bands 6, 7, 8, 8a, and 11 (a2) are from an image acquired on April 29, 2017. (b) Extractions from band 5 (b1), and bands 6, 7, 8, 8a and 11 (b2) are from an image acquired on June 8, 2017. (c) Extractions from band 5 (c1), and bands 6, 7, 8, 8a, and 11 (c2) from an image acquired on August 17, 2019. (d) Extractions from band 5 (d1), and bands 6, 7, 8, 8a and 11 (d2) of image acquired on May 3, 2020.

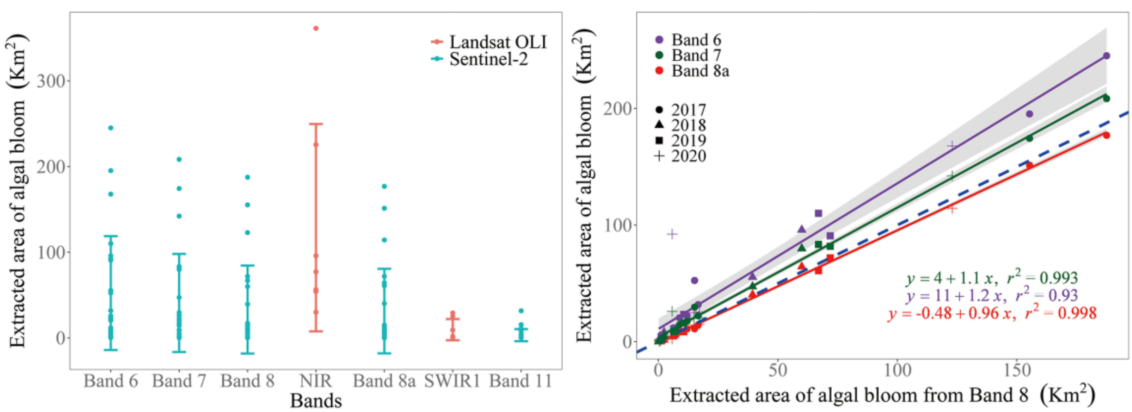

(a) (b)

Fig. 5. Comparison of algal bloom extraction among different bands. (a). Error bar graph for extracted algal bloom area of NIR, red-edge bands and first shortwave infrared band of sentinel-2 MSI and Landsat OLI images acquired during 2017–2020. (b) Comparison between the area of algal bloom extraction from NIR and red-edge bands of sentinel-2 MSI images acquired during 2017–2020 (the blue dashed line is 1:1).

III. Results

A. Extraction of Algal Blooms From Sentinel-2 MSI and Landsat OLI Images

Among all NIR, red-edge, and SWIR1 bands from sentinel-2 MSI images, the extracted area of high–high clusters in band 5 was the largest, covering both algal bloom regions and turbid water areas (see Fig. 4; more example extractions in supplementary material b), which is significantly different from the area extracted from other bands (ANOVA $P < 0.05$). All the other red-edge bands (6, 7, and 8a) showed similar performance for algal bloom extraction as the NIR band (sentinel-2 MSI band 8; Fig. 4); also shown by an ANOVA and Tukey HSD test ($P > 0.05$, Fig. 5). More algal blooms extracted from bands 8, 7, and 6 are near the boundary of the spatial extents of the algal blooms from band 8a (see Fig. 4). The extraction from SWIR1 band shows the spatial extents of algal blooms with the highest density [see Fig. 4(a1), (a2), (d1), and 4(d2)]. The extraction from NIR band (Landsat OLI) covers the algal bloom region, while the extraction from SWIR1 band only captures highly dense blooms (see Fig. 6). Landsat OLI images captured two severe bloom events [see Figs. 6(a) and 6(b)], which are consistent with the results from two extractions of the largest algal blooms from 2017 to 2020 [see Fig. 5(a)].

Algal bloom extraction from NIR and SWIR1 of Landsat OLI imagery is similar to the results from sentinel-2 MSI imagery by comparing images from the same date [see Fig. 4(d) and 4(d2); and Figs. 6(d) and (d1)]. The extraction results were compared for Landsat OLI and sentinel-2 MSI data acquired on similar dates (Landsat images acquired on May 11, 2017, May 27, 2017, December 21, 2017, April 28, 2018, November 9, 2019, May 3, 2020 paired with sentinel-2 MSI images acquired on April 29, 2017, May 29, 2017, December 20, 2017, May 4, 2018, November 5, 2019, May 3, 2020). Only the extraction area of both images acquired on the same date (May 3, 2020) is near the 1:1 line [see Fig. 7(a)]. This is because the area and spatial

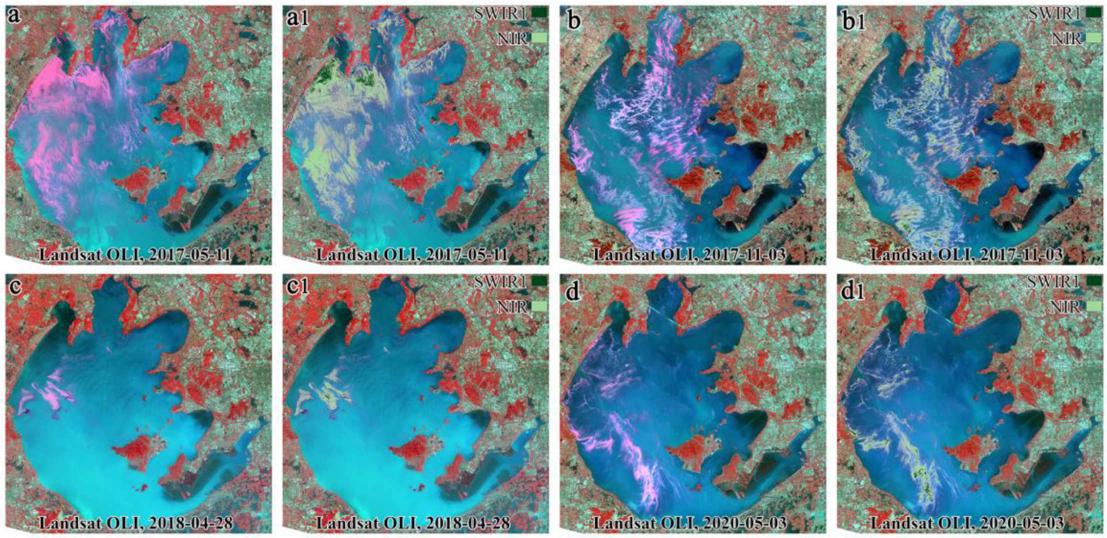

Fig. 6. Sample algal bloom extraction results from Landsat OLI images. (a) Extraction from NIR and SWIR1 band (a1) of image acquired in May 11, 2017. (b) Extraction from NIR and SWIR1 band (b1) of image acquired in November 3, 2017. (c) Extraction from NIR and SWIR1 band (c1) of image acquired in April 28, 2018. (d) Extraction from NIR and SWIR1 band (d1) of image acquired in 2020-05-03.

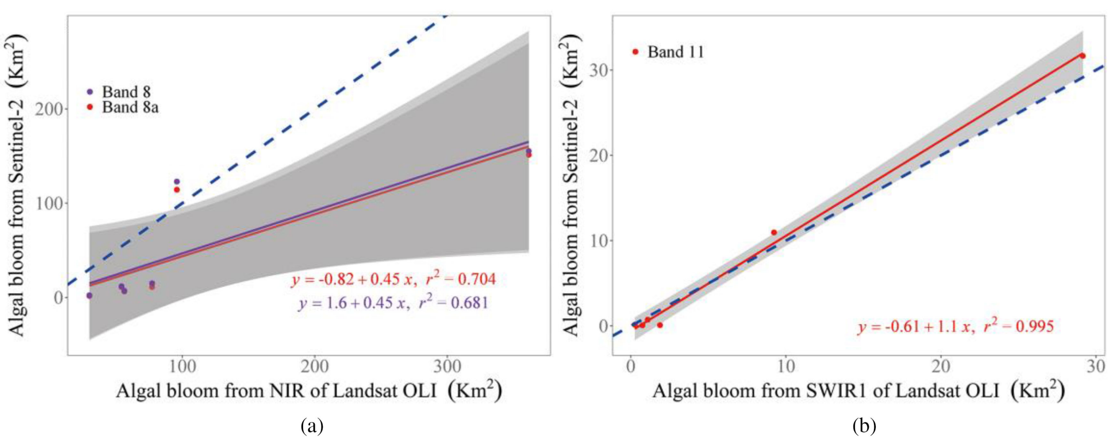

Fig. 7. Comparison of algal bloom extraction from the NIR band and first shortwave infrared (SWIR1) band between Landsat OLI and sentinel-2 MSI images. (a) Comparison of band 8a, band 8 of sentinel-2 MSI images and NIR of Landsat OLI images. (b) Comparison of SWIR1 bands of Landsat OLI and sentinel-2 MSI images (the blue dashed line is 1:1).

extent of algal blooms changes rapidly even within one or two days (see Fig. 8) and Landsat images captured larger algal bloom than sentinel-2 MSI images due to the acquisition dates. The extraction area from the SWIR1 band from both satellite images is similar [see Fig. 7(b)].

B. Validation of the Extracted Algal Bloom With MODIS FAI Data

The FAI value of the extracted algal bloom area from SWIR1 band is significantly higher than that from NIR band [$P < 0.05$; Fig. 9(a)]. FAI of the extracted area from NIR band is also significantly higher than that of the unextracted area from MODIS data with FAI larger than -0.004 [$P < 0.05$; Fig. 9(a)], and this FAI threshold (> -0.004) was considered as the threshold for mapping algal blooms from MODIS images in Lake Taihu [71]. The extracted algal bloom from the NIR band was considered to be level 1 (L1; interpreted as moderate algal bloom in this study), while that from SWIR1 was level 2 (L2; interpreted as severe algal bloom in this study) and the unextracted area with FAI larger than -0.004 was marked as level 0 (L0). After the FAI values of the three severity levels were extracted [see Fig. 9(a)], moderate and severe algal bloom thresholds were calculated based on the criteria of "median $+$ 1.5$\times$interquartile range" of L0 and L1 to avoid statistical outliers [see Fig. 9(a)]. The two thresholds were then used to extract moderate and severe algal bloom regions from MODIS FAI images to validate the extractions from sentinel-2 MSI and Landsat OLI images (i.e., both satellite images were paired with MODIS images based on the same acquisition date). The extracted moderate and

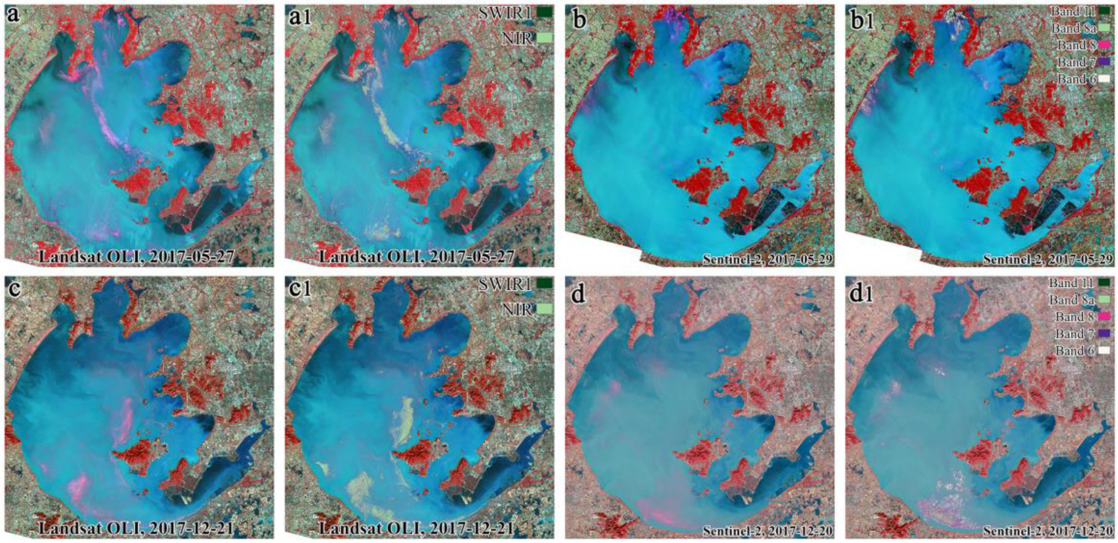

Fig. 8. Comparison of algal bloom occurrence on similar acquisition dates from Landsat OLI and sentinel-2 MSI images. (a) Algal bloom extraction from NIR and SWIR1 bands (a1) of Landsat image acquired in May 27, 2017. (b) Algal bloom extraction from band 6, 7, 8, 8a, and 11 (b1) of sentinel-2 MSI image acquired in May 29, 2017. (c) Algal bloom extraction from NIR and SWIR1 band (c1) of Landsat image acquired in December 21, 2017. (d) Algal bloom extraction from bands 6, 7, 8, 8a, and 11 (d1) of sentinel-2 MSI image acquired in December 20, 2017.

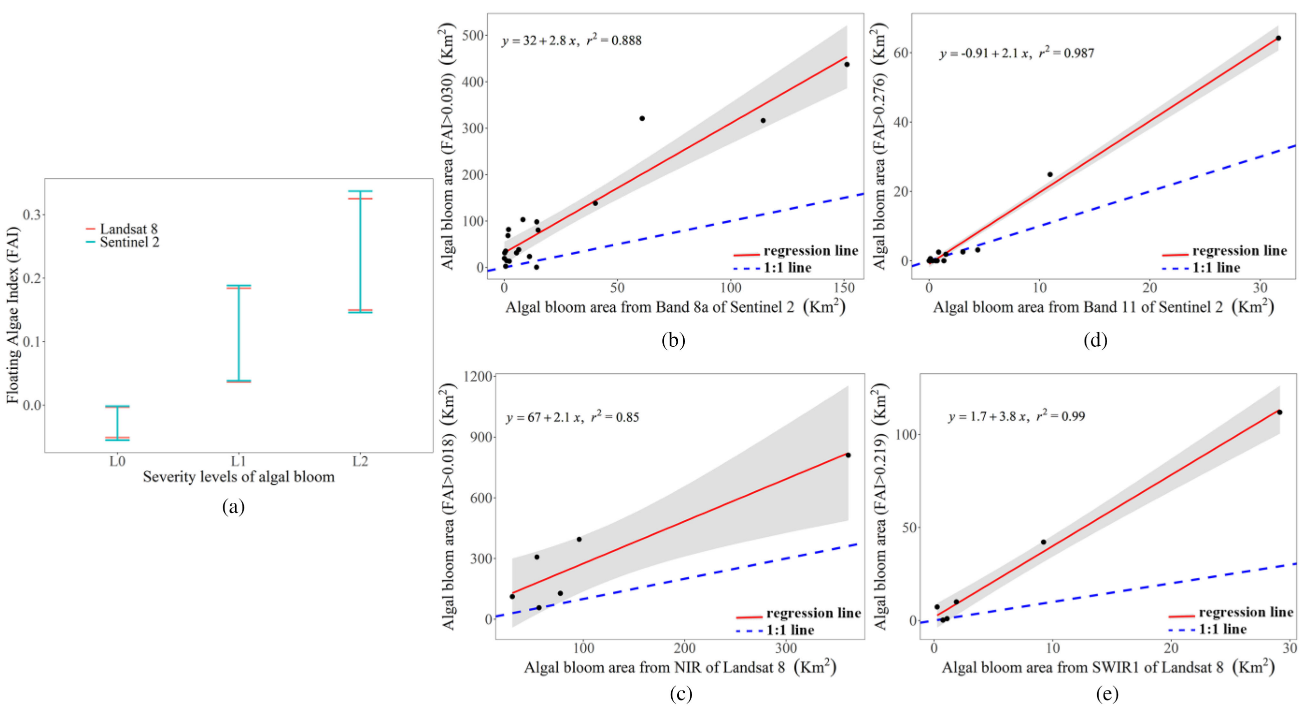

Fig. 9. Validation of algal bloom extraction from sentinel-2 MSI and Landsat images based on MODIS derived FAI. (a) Error bar graph of FAI of unextracted area with FAI larger than −0.004 (L0), extracted area from NIR band (L1), extracted area from first SWIR1 band (*L*2). (b) Validation of extracted algal bloom area from sentinel-2 MSI band 8a with the area of MODIS FAI larger than 0.03. (c) Validation of extracted algal bloom area from Landsat OLI NIR with the area of MODIS FAI larger than 0.0018. (d) Validation of extracted algal bloom area from sentinel-2 MSI band 11 with the area of MODIS FAI larger than 0.276. (e) Validation of extracted algal bloom area from Landsat OLI SWIR1 with the area of MODIS FAI larger than 0.219.

severe algal blooms from both satellite images are significantly correlated with the MODIS FAI, but were underestimations compared to MODIS (see Fig. 9; see the comparison of extracted spatial extents of algal blooms from both satellite images and MODIS images in the supplementary material D). The spectral characteristics of the extracted moderate and severe algal blooms also indicates that the severe algal blooms show significantly high reflectance in both NIR (including bands 6, 7, 8, and 8a for sentinel-2 MSI images) and SWIR1 bands for both sentinel-2 MSI and Landsat OLI images (see Fig. 10). Oyama, *et al.* [52]'s

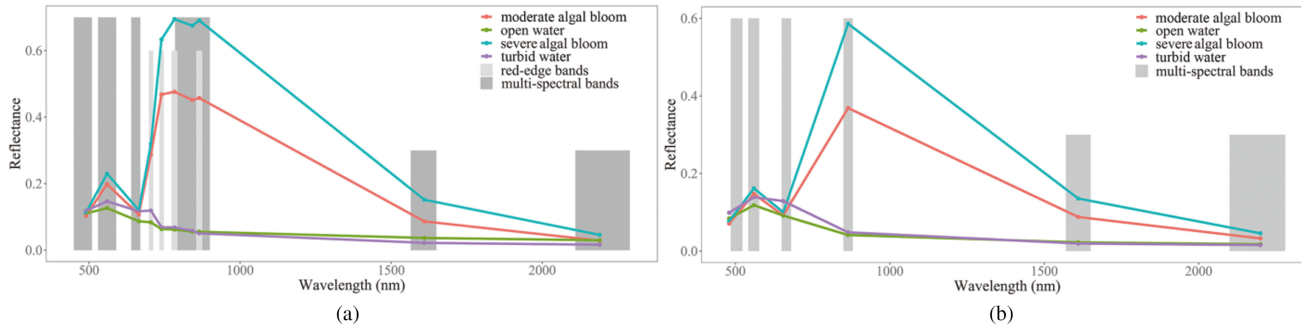

Fig. 10. Spectral characteristics of severe algal blooms, algal blooms, turbid water and open water in Lake Taihu extracted from sentinel-2 MSI and Landsat OLI imagery. (a) Spectra extracted from the sentinel-2 MSI images, (b) Spectra extracted from the Landsat OLI images.

research using Landsat ETM^+ in Japan indicates that FAI in the range 0–0.1 represents moderate algal blooms (level 3 and level 4 of VCI characterized by surface scums or thin film), which is consistent of our extraction from NIR bands. However, Oyama *et al.* [52]'s findings show that FAI is unable to identify level 5 (thick surface mat) and level 6 (hyperscum) of cyanobacterial blooms. Therefore, the extraction results of SWIR1 might only represent severe algal blooms with high surface scum density instead of a severe algal bloom in ecological context.

C. Temporal and Spatial Dynamics of Algal Blooms During 2017–2020

Multiple algal blooms were detected throughout the study period using both remote sensing platforms and with variable severity, duration (see Fig. 11) and spatial extent (see Fig. 6). During 2017 to 2020, the largest bloom outbreak occurred in 2017; the largest detected by both satellites was 361.37 km^2 on May 11, 2017 with five large algal bloom outbreaks detected in 2017 [see Fig. 11(a)]. The smaller bloom during July 28, 2017 to August 17, 2017 with an extracted maximum area of 70.61 km^2 was detected with low confidence due to cloud-obscured images [see Fig. 11(a)]. Hence, this algal bloom may have been larger.

The mildest outbreaks of algal bloom in the study period were detected in 2018 [see Fig. 11(b)]. The largest bloom outbreak lasted more than two months with a maximum area of 64.32 km^2. Two other smaller and briefer blooms were detected that year [see Fig. 11(a)]. In 2019, three algal blooms were detected, and five algal blooms were detected in 2020; all milder than in 2017 [see Fig. 11(c) and (d)].

Moderate algal blooms can cover up to 15% of the area of the largest section of Lake Taihu (section 6: 1367 km^2) and severe blooms cover up to 2.5% of its area [see Fig. 12(a) and (b)]. The smallest section (see section 1: 193.63 km^2) had a greater percentage area of moderate and severe blooms [see Fig. 12(a) and (b)] than the larger sections (section 2: 174.44 km^2, section 3: 239.83 km^2, and section 5: 228.21 km^2). Sections 3 and 5, regions originally dominated by aquatic vegetation, had the mildest algal bloom outbreaks compared to the other three, but were nevertheless subject to some algal bloom outbreaks [see Fig. 12(a) and (b)]. The *in situ* measured Chl*a* also show section 1 and 6 have high concentration of Chl*a*, section 2 has moderate concentration of Chl*a*, and section 5 and 3 have low concentration of Chl*a*, which is consistent with the estimate cover percentage of moderate algal blooms (Fig. 12c and 12b). Section 2 had few severe algal blooms [see Fig. 12(b) but had many blooms of lesser severity [see Fig. 12(a)] likely due to serious anthropologic pollution. Section 4 was not included for algal bloom extraction in this article because it is dominated by submerged vegetation and anthropologic disturbance from both dynamic land cover changes and fisheries.

IV. Discussion

A Advantages and Limitations of LISA for Algal Bloom Mapping

This qualitative approach, based on the concept of LISA, automatically extracts algal blooms from satellite images. Most remote sensing classification methods (e.g., threshold methods based on spectral indices, decision trees, pixel-based classification, objected oriented classification, and machine learning) require training samples to develop classification rules and criteria or post classification solutions to improve classification accuracy [33], [42], [72]. However, methods that rely on human judgment lack temporal consistency for images acquired on different dates. Previous studies have also shown that spatial weights (i.e., important parameters for spatial autocorrelation analysis) improve the temporal consistency for remote sensing classifications [54]. This method eliminates inconsistency found in other pixel-based classification methods as it correlates each pixel with its neighbors. Another advantage of the autocorrelation method comes from automation and batch processing. Dynamic algal blooms require rapid monitoring with the ability to rapidly batch-process high data volumes. We found that this automatic method has the capacity to extract algal bloom information from both sentinel-2 MSI and Landsat OLI images with high accuracy, temporal consistency and batch processing ability. It is particularly effective at extracting spatial extents that have been affected by similar phenomena as neighboring pixels [55]. It is also effective at distinguishing relatively homogeneous land cover types with higher (high–high clusters) or low (low–low clusters) spectral reflectance and is suitable for extracting algal

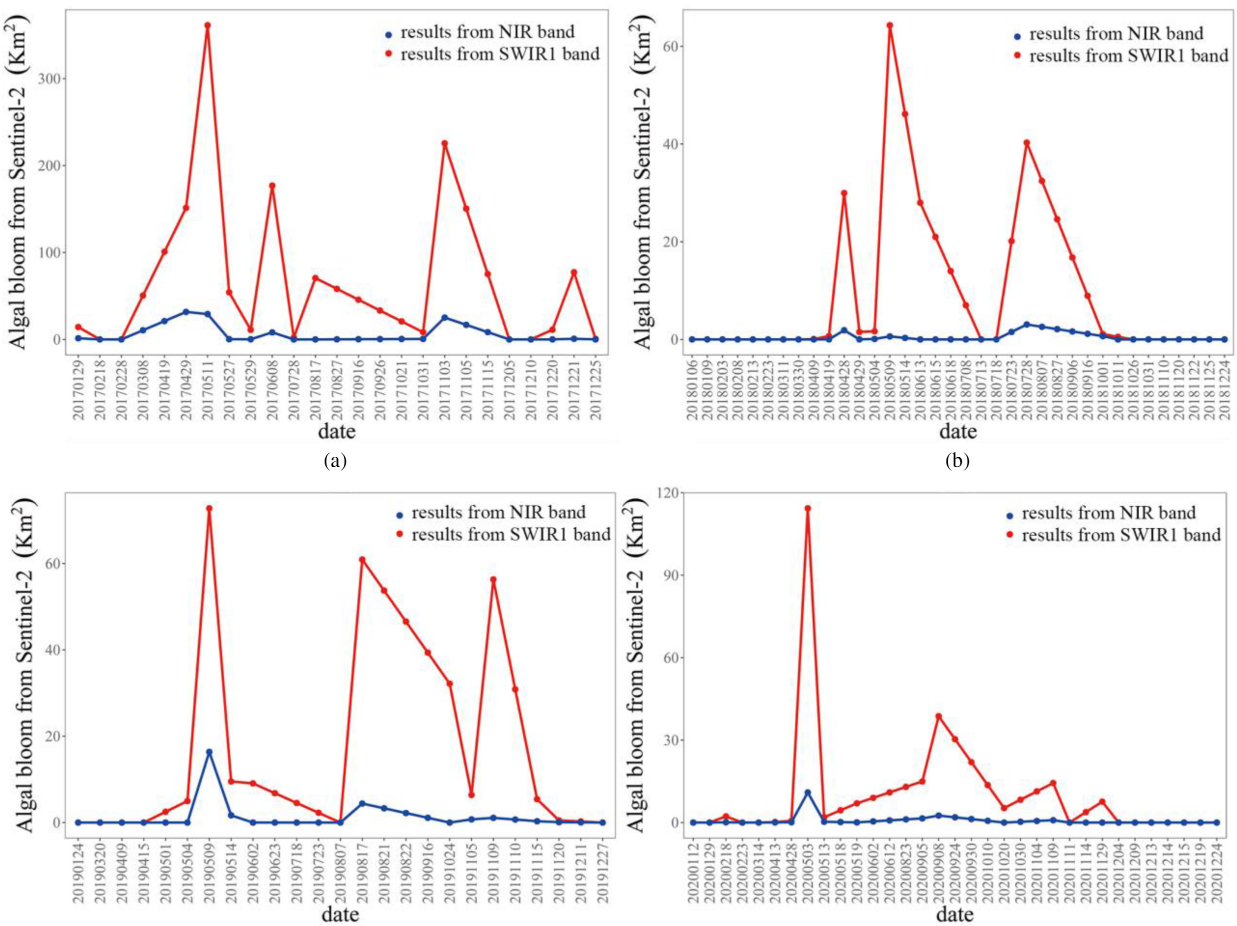

Fig. 11. Temporal dynamics of the extracted area of algal blooms in Lake Taihu in (a) 2017, (b) 2018, (c) 2019, and (d) 2020. In each panel, the graphs show the extracted area of algal blooms from band 8a of sentinel-2 MSI and NIR band from Landsat OLI images (red dots and line) and band 11 of sentinel-2 MSI and first SWIR1 band of Landsat OLI images (blue line and dots).

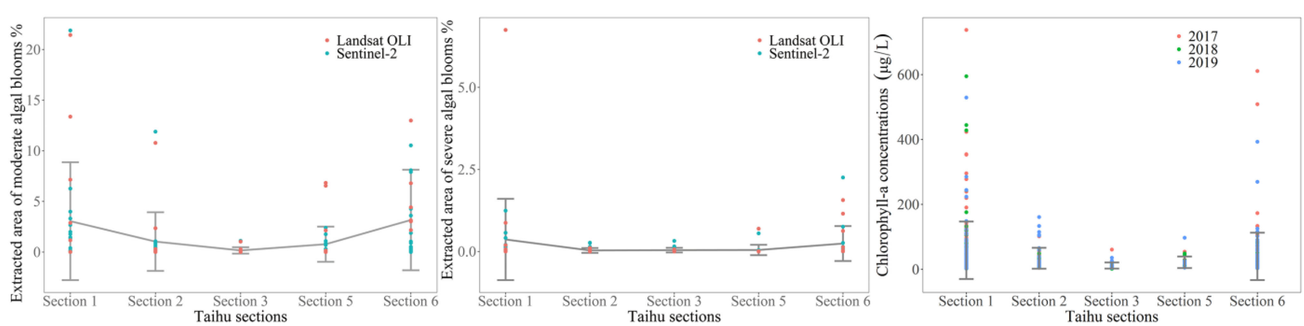

Fig. 12. Algal bloom outbreaks in different sections of Lake Taihu. (a) Extracted area of moderate algal blooms from the all cloud-free images divided by the area of the sections. (b) Extracted area of severe algal blooms from all the cloud-free images divided by the area of the sections. (c) *In situ* measured Chl*a* from different sections in Lake Taihu.

blooms from waters using the NIR wavelength region [see Figs. 3 and 10].

The limitation of this approach is that it is difficult to distinguish algal blooms from other land cover types that also have significantly higher reflectance than open water. This included islands, bridges, aquatic vegetation and river plumes [55]. Therefore, it needs to use the unique spectral signals among spectral bands for various land cover types in the Lake Taihu area. For this reason, selection of spectral bands for extracting the spatial extents of algal blooms is very important (see "C. Algal Bloom Extraction Among Spectral Bands" in the section of "IV. DISCUSSION"). The effects of other land cover types with high reflectance values were minimized with accurate surface water extraction that masked those features, retaining only open water regions. We have previously shown that the SWIR2 band performs well to map open surface water with high turbidity or algal bloom coverage, but with islands, bridges and aquatic vegetation excluded [69].

We were careful to identify the error sources in our method, including sensitivity to image quality and spatial resolution that reduced extraction accuracy from both image platforms. Cloud cover is the main image quality issue for bloom extraction as clouds with high reflectance can be extracted as algal blooms [see Fig. 4(b) and (b2)]. Thin clouds were only extracted from bands in the red-edge and NIR wavelength region [see Fig. 4(b1) and (b2)], while thick clouds were extracted by all the studied bands at the red-edge, NIR and SWIR1 wavelength regions (Supplementary C). If both algal blooms and thick cloud cover were present in the images, bands in the red-edge and NIR wavelength region extracted both moderate algal blooms and thick cloud while SWIR1 bands only extracted thick clouds and severe algal blooms (supplementary material C: sentinel-2 MSI image acquired in August 17, 2017 and Landsat OLI image acquired in September 8, 2020). Hence, our results point to ways to manage this error source using a diversity of bands and image platforms.

Another image quality issue that might affect extraction accuracy using spatial analysis is "salt and pepper" effects [69]. However, this was not found in our study because Landsat OLI and sentinel-2 MSI images with geomatics and atmospheric correction have high image quality that overcome the issue. Spatial resolution of satellite images also impacts the extraction area, mainly at the edge or boundary between algal blooms and water. Different spatial resolution may result in variable homogeneity, which affects spatial autocorrelation. As well, the extracted areas were not uniform due to different pixel sizes. Hence, the spatial extent of the extracted algal blooms from sentinel-2 MSI and Landsat OLI images acquired in the same date [May 3, 2020, Figs. 4(d2) and 6(d1)], calculated different algal bloom areas [see Fig. 7(a)]. This was caused by differing spatial resolution.

B. Comparison of Landsat OLI and Sentinel-2 MSI Images

It is a challenge to compare the extraction results of algal blooms from sentinel-2 MSI images and Landsat OLI images. Algal blooms change dramatically over a few hours; therefore, images acquired even on adjacent dates may not be comparable (see Fig. 8). Indeed, the principal reason for nonuniform of algal bloom cover on similar dates (see Fig. 8) is aquatic management; the salvaging of algal blooms. Salvaged algal blooms amounted to 45.97 million tons in May 2017 for instance, affecting the detected intensity and comparison between image platforms. During the study period in 2017–2020, most Landsat OLI images captured more intense and larger algal bloom outbreaks than sentinel-2 MSI images, especially when images were on similar dates (see Fig. 7). However, the comparison of the two satellite images from the same dates show the opposite; the extracted bloom area from NIR region of sentinel-2 MSI is larger than that of Landsat OLI image [see Figs. 4(d2) and 6(d1); NIR band of Landsat OLI image extracted 95.93 km^2; NIR band and band 8a of sentinel-2 MSI images extracted 122.92 and 114.32 km^2, respectively). This suggests that, in addition to the effects of spatial resolution, inconsistent results may stem from sensor design (i.e., wavelength position and band width) for NIR bands in Landsat-8 and sentinel-2 MSI satellites (see Fig. 10).

Compared to MODIS images based on FAI thresholds, the extractions of algal blooms were underestimated on both sentinel-2 MSI and Landsat OLI platforms (see Fig. 9). However, the spatial extent of the extracted moderate and severe algal blooms was consistent with the extractions from MODIS FAI images (see supplementary D). One reason for the underestimation is the large gap in spatial resolution of both satellite images and MODIS. Because images with coarse spatial resolution have issues with mixed pixels, the threshold of FAI may need to be set lower to detect and map algal blooms. This may also be the reason for lower FAI thresholds of Landsat OLI images than sentinel-2 MSI images (see supplementary D). Regardless, these effects and the difference in transit time of MODIS and the other two satellites contribute to the inconsistency of algal bloom extractions.

C. Algal Bloom Extractions Among Spectral Bands

Previous studies on Lake Taihu indicate that visible bands are highly influenced by turbidity [69]. This can make them unsuitable for water mapping as water-leaving radiance is dominated by particulate scattering properties instead of absorption in highly turbid water [73]. The spectral characteristics from the USGS library show that reflectance of visible bands varies with water turbidity (see Fig. 3). Turbid water has higher reflectance in the visible wavelength region (see Fig. 3), which influences algal bloom extraction from visible bands. The spectral signals from both sentinel-2 MSI and Landsat OLI images also suggest that there is not much separation between turbid water and algal blooms in the visible wavelength region (see Fig. 10). Oyama *et al.* [3] indicated that cyanobacterial blooms and water are indistinguishable in three visible bands. Even though the reflectance of algal blooms in band 5 of sentinel-2 MSI images is higher than that in turbid water, its capacity for algal bloom extraction is much lower than in the NIR and SWIR1 wavelength regions [see Fig. 10(a)]. This is because turbid water also has high reflectance in band 5 [see Fig. 10(a)], and its reflectance varies across suspended sediment concentrations.

Research has also shown that algal bloom reflectance reaches its maximum at around 700 nm (band 5 wavelength range in sentinel-2 MSI images: 698–713 nm) due to the high concentration of phytoplankton in the water column and surface algal scum [2]. However, sediment resuspension is a common event in Lake Taihu due to its shallow depth and flat lakebed, resulting in consistent, year-round turbidity (average and maximum concentration of suspended particular matter is over 50 and 300 $mg \cdot L^{-1}$). This results in high reflectance of turbid water in band 5 (see Fig. 10) [63], [74], [75].

Except in the visible bands and band 5 of sentinel-2 MSI, the turbid water in Lake Taihu have similar spectral signals as clear open water (see Fig. 10), where reflectance decreases with increasing wavelength [76]. Therefore, water with low reflectance clusters in NIR, SWIR1 and SWIR2 bands (see Fig. 10), have often been used for water mapping studies [40], [77]. Becker *et al.* [78] also found that the NIR region is superior to the visible region for mapping algal blooms in water. Algal blooms have significantly higher reflectance in NIR and SWIR1 regions than clear or turbid waters. They do not differ significantly in the SWIR2 band (see Fig. 10). Thus, SWIR2 has little potential to extract algal blooms from water, consistent with previous research [69]. Both moderate and severe algal blooms have significantly higher reflectance than turbid or clear water in NIR and part of the red-edge wavelength regions (bands 6, 7, 8a, and 8 for sentinel-2 MSI images and NIR for Landsat OLI images; Fig. 10). Therefore, the extraction results from those bands captured the majority of the spatial extent of algal bloom outbreaks (see Figs. 4 and 6). The extracted algal bloom area from those bands was slightly different due to different wavelength regions, band widths and spatial resolutions (see Figs. 5 and 10). Oyama *et al.* [3] also showed that lake water and algal blooms are distinguishable in the NIR region but not the SWIR2 region. In the SWIR1 wavelength region, eutrophic water has large reflectance gaps compared to clear or turbid water (see Fig. 10); thus, only severe algal blooms were detectable (see Figs. 4 and 6). Previous research indicated that both SWIR1 and SWIR2 bands are able to distinguish cyanobacterial blooms and macrophytes, but are unable to discriminate cyanobacterial blooms and lake water [3]. Lake Taihu, as a shallow fluvial lake, is characterized by the coexistence of phytoplankton and macrophytes [79]. In this article, the severe algal blooms extracted from the SWIR1 band had similar reflectance in SWIR2 as turbid and clear water and algal blooms (see Fig. 10). This suggested that the extracted severe algal blooms might not be misclassified macrophytes.

D. Monitoring Algal Blooms Using Images With Long Revisiting Intervals

It is a challenge to analyze the duration and frequency of algal bloom outbreaks using optical satellite images with long revisiting intervals and cloud effects. Therefore, we visibly checked all images, including those obscured by cloud, for algal bloom occurrence. sentinel-2 MSI, with two satellites (A and B), has a revisiting interval of five days. A continuous dataset of algal bloom outbreaks from 2017 to 2020 can be created by adding Landsat OLI results. The interpolation data for missing algal bloom values due to cloud cover may not represent the true bloom area, but the temporal dataset, with interpolation values, can predict the duration and frequency of bloom outbreaks. Previous studies have also used satellite images (e.g., MERIS) to identify dates of cyanobacterial bloom occurrence and used images with higher spatial resolution (e.g., Landsat OLI) to map the spatial distribution of algal blooms [39].

Previous studies of inland lakes in North America and Italy indicate that algal blooms normally occur in summer or early autumn [9], [30], [35], [37], [39]. However, algal blooms in Lake Taihu occurred in spring, summer and autumn during 2017–2020, with even small outbreaks in winter (2017 and 2020; Fig. 11). Other monitoring at Lake Taihu indicated that algal blooms mainly occur from May to September [59]. The results of this study indicate five continuous outbreaks from February 28, 2017 to December 25, 2017 [about ten months, Fig. 11(a)], three from April 9, 2018 to October 26, 2018 [about 6.5 months, Fig. 11(b)], three from April 15, 2019 to November 20, 2019 [about seven months, Fig. 11(c)], and four major continuous outbreaks (except the outbreak from January 29, 2020 to February 23, 2020, Fig. 11(d)] from April 13, 2020 to December 4, 2020 [about 7.5 months, Fig. 11(d)]. Starting dates of algal blooms in Lake Taihu have been found to be very early (average phenological starting date was 29.9 days during 2003–2017) [80]. Compared to the large algal bloom that occurred on Erhai Lake with a coverage of 150 km^2 in 1996 [6], the largest algal bloom outbreak covered 361.37 km^2 in May 5 2017 [see Fig. 11(a)].

Compared to the temporal changes of *in situ* measured Chl*a* data in 2017–2019 (supplementary D), the frequency and duration of extracted algal blooms (see Fig. 11) were not exactly consistent with Chl*a* concentration. Chl*a* concentration measured once a month is insufficient to indicate the frequency and occurrence duration of all the algal blooms (supplementary D) because they rapidly appear and disappear within a few days, or even within a few hours [12], [37]. However, the extracted results from sentinel-2 MSI and Landsat OLI images show some agreement with the field measured Chl*a* concentration (supplementary D) when the data collection dates were similar with image acquiring dates. The largest algal bloom extracted in May 11, 2017 from the images was consistent with highest Chl*a* concentration (i.e., total concentration of all the samples measured in May 15, 2017; supplementary D). However, the extraction of algal blooms from the images did not capture the highest spatial extents of two outbreaks compared to the Chl*a* data [i.e., the algal blooms occurred in the summer of 2017 and 2019; Fig. 11(a) and (c); supplementary D]. This indicates the combination of sentinel-2 MSI and Landsat OLI (i.e., with the revisit frequency of 2–3 days) might still miss some temporal characteristics of algal bloom outbreaks due to cloud cover. More work (e.g., integrating synthetic aperture radar data [81]) will be needed to improve the temporal resolution for images with high spatial resolution to monitor algal blooms in inland waters wherein rain and clouds are frequent.

V. Conclusion

Based on a methodology developed using the LISA concept, NIR and red-edge bands (bands 6, 7, 8, and 8a from sentinel-2 MSI images or band 5 from Landsat OLI images) are capable of measuring the spatial distribution of moderate algal blooms in shallow Lake Taihu. However, the other red-edge band (band 5 of sentinel-2 MSI), in contrast to previous studies, performed poorly for algal bloom detection due to turbidity and high concentrations of suspended matter. This approach may be applied to map the spatial distribution of algal blooms using a combination of satellite platforms (i.e., band configuration in

NIR, red-edge or SWIR1 wavelength regions) with automation and batch-processing capacity.

The temporal resolution of the combination of Landsat OLI and sentinel-2 MSI images would miss some important temporal characteristics of surface algal blooms in the summer time due to cloud effects on the images in Lake Taihu.

Acknowledgment

The authors would also like to thank Taihu Laboratory for Lake Ecosystem Research for providing *in situ* data.

References

[1] K. Shi, Y. Zhang, B. Qin, and B. Zhou, "Remote sensing of cyanobacterial blooms in inland waters: present knowledge and future challenges," *Sci. Bull.*, vol. 64, no. 20, pp. 1540–1556, Oct. 2019.

[2] M. Nazeer, M. S. Wong, and J. E. Nichol, "A new approach for the estimation of phytoplankton cell counts associated with algal blooms," *Sci. Total Environ.*, vol. 590, pp. 125–138, Jul. 2017.

[3] Y. Oyama, B. Matsushita, and T. Fukushima, "Distinguishing surface cyanobacterial blooms and aquatic macrophytes using landsat/TM and ETM plus shortwave infrared bands," *Remote Sens. Environ.*, vol. 157, pp. 35–47, Feb. 2015.

[4] L. Aubriot *et al.*, "Assessing the origin of a massive cyanobacterial bloom in the Rio de la Plata (2019): Towards an early warning system," *Water Res.*, vol. 181, Aug. 2020, Art. no. 115944.

[5] J. S. Beckler, E. Arutunian, T. Moore, B. Currier, E. Milbrandt, and S. Duncan, "Coastal harmful algae bloom monitoring via a sustainable, sail-powered mobile platform," *Frontiers Marine Sci.*, vol. 6, Oct. 2019, Art. no. 587.

[6] W. Tan, P. Liu, Y. Liu, S. Yang, and S. Feng, "A 30-year assessment of phytoplankton blooms in Erhai Lake using Landsat imagery: 1987 to 2016," *Remote Sens.*, vol. 9, no. 12, Dec. 2017, Art. no. 1265.

[7] V. Klemas, "Remote sensing of algal blooms: An overview with case studies," *J. Coastal Res.*, vol. 28, no. 1A, pp. 34–43, Jan. 2012.

[8] P. Wu, Y. Lu, Y. Lu, J. Dai, and T. Huang, "Response of the photosynthetic activity and biomass of the phytoplankton community to increasing nutrients during cyanobacterial blooms in Meiliang Bay, Lake Taihu," *Water Environ. Res.*, vol. 92, no. 1, pp. 138–148, Jan. 2020.

[9] M. Y. Grishin *et al.*, "Laser remote sensing of an algal bloom in a freshwater reservoir," *Laser Phys.*, vol. 26, no. 12, Dec. 2016, Art. no. 125601.

[10] W. Zhang *et al.*, "Phenotype changes of cyanobacterial and microbial distribution characteristics of surface sediments in different periods of cyanobactErial blooms in Taihu Lake," *Aquatic Ecol.*, vol. 54, no. 2, pp. 591–607, Jun. 2020.

[11] J. Ma *et al.*, "Spatiotemporal pattern of gypsum blooms in the Salton Sea, California, during 2000-2018," *Int. J. Appl. Earth Observ. Geoinf.*, vol. 89, Jul. 2020, Art. no. 102090.

[12] M. Bresciani *et al.*, "Monitoring blooms and surface accumulation of cyanobacteria in the Curonian Lagoon by combining MERIS and ASAR data," *Remote Sens. Environ.*, vol. 146, pp. 124–135, Apr. 2014.

[13] T. Zhang, H. Hu, X. Ma, and Y. Zhang, "Long-term spatiotemporal variation and environmental driving forces analyses of algal blooms in Taihu Lake based on multi-source satellite and land observations," *Water*, vol. 12, no. 4, Apr. 2020, Art. no. 1035.

[14] I. Ogashawara, L. Li, and M. J. Moreno-Madrinan, "Slope algorithm to map algal blooms in inland waters for Landsat 8/Operational Land Imager images," *J. Appl. Remote Sens.*, vol. 11, no. 1, Dec. 2016, Art. no. 012005.

[15] P. R. Hill, A. Kumar, M. Temimi, and D. R. Bull, "HABNet: Machine learning, remote sensing-based detection of harmful algal blooms," in *Proc. IEEE J. Sel. Topics Appl. Earth Observ. Remote Sens.*, 2020, pp. 3229–3239.

[16] J. Li *et al.*, "Satellite-based estimation of column-integrated algal biomass in nonalgae bloom conditions: A case study of Lake Chaohu, China," *IEEE J. Sel. Topics Appl. Earth Observ. Remote Sens.*, vol. 10, no. 2, pp. 450–462, Feb. 2017.

[17] Y. Tian and M. Huang, "An integrated web-based system for the monitoring and forecasting of coastal harmful algae blooms: Application to Shenzhen city, China," *J. Marine Sci. Eng.*, vol. 7, no. 9, Sep. 2019, Art. no. 314.

[18] J. Shin, S. M. Kim, K. Kim, and J. - H. Ryu, "Quantification of Margalefidinium polykrikoides blooms along the south coast of Korea using airborne hyperspectral imagery," *Remote Sens.*, vol. 12, no. 15, Aug. 2020, Art. no. 2463.

[19] R. Bolpagni, M. Bresciani, and S. Fenoglio, "Aquatic biomonitoring: Lessons from the past, challenges for the future," *J. Limnol.*, vol. 76, no. s1, pp. 1–4, 2017.

[20] Z. Qiu, Z. Li, M. Bilal, S. Wang, D. Sun, and Y. Chen, "Automatic method to monitor floating macroalgae blooms based on multilayer perceptron: case study of Yellow Sea using GOCI images," *Opt. Exp.*, vol. 26, no. 21, pp. 26810–26829, Oct. 2018.

[21] S. Karki, M. Sultan, R. Elkadiri, and T. Elbayoumi, "Mapping and forecasting onsets of harmful algal blooms using MODIS data over coastal waters surrounding Charlotte County, Florida," *Remote Sens.*, vol. 10, no. 10, Oct. 2018, Art. no. 1656.

[22] M. Sayers, G. L. Fahnenstiel, R. A. Shuchman, and M. Whitley, "Cyanobacteria blooms in three eutrophic basins of the Great Lakes: A comparative analysis using satellite remote sensing," *Int. J. Remote Sens.*, vol. 37, no. 17, pp. 4148–4171, 2016.

[23] A. El-Alem, K. Chokmani, I. Laurion, S. E. El-Adlouni, S. Raymond, and C. Ratte-Fortin, "Ensemble-based systems to monitor algal bloom with remote sensing," *IEEE Trans. Geosci. Remote Sens.*, vol. 57, no. 10, pp. 7955–7971, Oct. 2019.

[24] M. Ghanea, M. Moradi, and K. Kabiri, "A novel method for characterizing harmful algal blooms in the Persian Gulf using MODIS measurements," *Adv. Space Res.*, vol. 58, no. 7, pp. 1348–1361, Oct. 2016.

[25] V. C. Andreo, A. I. Dogliotti, and C. B. Tauro, "Remote sensing of phytoplankton blooms in the continental shelf and shelf-break of Argentina: Spatio-temporal changes and phenology," *IEEE J. Sel. Topics Appl. Earth Observ. Remote Sens.*, vol. 9, no. 12, pp. 5315–5324, Dec. 2016.

[26] R. Y. Setiawan and A. Habibi, "Satellite detection of summer chlorophyll-a bloom in the Gulf of Tomini," *IEEE J. Sel. Topics Appl. Earth Observ. Remote Sens.*, vol. 4, no. 4, pp. 944–948, Dec. 2011.

[27] P. Shanmugam, M. Suresh, and B. Sundarabalan, "OSABT: An innovative algorithm to detect and characterize ocean surface algal blooms," *IEEE J. Sel. Topics Appl. Earth Observ. Remote Sens.*, vol. 6, no. 4, pp. 1879–1892, Aug. 2013.

[28] M. Tao, H. Duan, Z. Cao, S. A. Loiselle, and R. Ma, "A hybrid EOF algorithm to improve MODIS cyanobacteria phycocyanin data quality in a highly Turbid Lake: Bloom and nonbloom condition," *IEEE J. Sel. Topics Appl. Earth Observ. Remote Sens.*, vol. 10, no. 10, pp. 4430–4444, Oct. 2017.

[29] R. Elkadiri *et al.*, "Development of a coupled spatiotemporal algal bloom model for coastal areas: A remote sensing and data mining-based approach," *IEEE J. Sel. Topics Appl. Earth Observ. Remote Sens.*, vol. 9, no. 11, pp. 5159–5171, Nov. 2016.

[30] Q. Xing and C. Hu, "Mapping macroalgal blooms in the Yellow Sea and East China Sea using HJ-1 and Landsat data: Application of a virtual baseline reflectance height technique," *Remote Sens. Environ.*, vol. 178, pp. 113–126, Jun. 2016.

[31] J. Chen and W. Quan, "Using Landsat/TM imagery to estimate nitrogen and phosphorus concentration in Taihu Lake, China," *IEEE J. Sel. Topics Appl. Earth Observ. Remote Sens.*, vol. 5, no. 1, pp. 273–280, Feb. 2012.

[32] E. M. Isenstein, A. Trescott, and M. - H. Park, "Multispectral remote sensing of harmful algal blooms in Lake Champlain, USA," *Water Environ. Res.*, vol. 86, no. 12, pp. 2271–2278, Dec. 2014.

[33] S. Lin, L. N. Novitski, J. Qi, and R. J. Stevenson, "Landsat TM/ETM+ and machine-learning algorithms for limnological studies and algal bloom management of inland lakes," *J. Appl. Remote Sens.*, vol. 12, no. 2, Apr. 2018, Art. no. 026003.

[34] S. Mishra, R. P. Stumpf, and A. Meredith, "Evaluation of RapidEye data for mapping algal blooms in inland waters," *Int. J. Remote Sens.*, vol. 40, no. 7, pp. 2811–2829, Apr. 2019.

[35] B. P. Page, A. Kumar, and D. R. Mishra, "A novel cross-satellite based assessment of the spatio-temporal development of a cyanobacterial hatinful algal bloom," *Int. J. Appl. Earth Observ. Geoinf.*, vol. 66, pp. 69–81, Apr. 2018.

[36] A. Drozd, P. de Tezanos Pinto, V. Fernandez, M. Bazzalo, F. Bordet, and G. Ibanez, "Hyperspectral remote sensing monitoring of cyanobacteria blooms in a large South American Reservoir: High- and medium-spatial resolution satellite algorithm simulation," *Mar. Freshwater Res.*, vol. 71, no. 5, pp. 593–605, 2020.

[37] M. Bresciani *et al.*, "Mapping phytoplankton blooms in deep subalpine lakes from Sentinel-2A and Landsat-8," *Hydrobiologia*, vol. 824, no. 1, pp. 197–214, Nov. 2018.

[38] S. Qing, A. Runa, B. Shun, W. Zhao, Y. Bao, and Y. Hao, "Distinguishing and mapping of aquatic vegetations and yellow algae bloom with Landsat satellite data in a complex Shallow Lake, China during 1986-2018," *Ecol. Indicators*, vol. 112, May. 2020, Art. no. 106073.

[39] M. Bresciani *et al.*, "Earth observation for monitoring and mapping of cyanobacteria blooms. Case studies on five Italian lakes," *J. Limnol.*, vol. 76, no. s1, pp. 127–139, 2017.

[40] L. R. Londe, E. M. L. M. Novo, C. Barbosa, and C. A. S. Araujo, "Water residence time affecting phytoplankton blooms: study case in Ibitinga Reservoir (Sao Paulo, Brazil) using Landsat/TM images," *Brazilian J. Biol.*, vol. 76, no. 3, pp. 664–672, Sep. 2016.

[41] C. Le, Y. Li, Y. Zha, D. Sun, C. Huang, and H. Lu, "A four-band semi-analytical model for estimating chlorophyll a in highly turbid lakes: The case of Taihu lake, China," *Remote Sens. Environ.*, vol. 113, no. 6, pp. 1175–1182, Jun 15 2009.

[42] M. J. Sayers *et al.*, "Satellite monitoring of harmful algal blooms in the Western Basin of Lake Erie: A 20-year time-series," *J. Great Lakes Res.*, vol. 45, no. 3, pp. 508–521, Jun. 2019.

[43] N. Torbick and M. Corbiere, "A multiscale mapping assessment of lake champlain cyanobacterial harmful algal blooms," *Int. J. Environ. Res. Public Health*, vol. 12, no. 9, pp. 11560–11578, Sep. 2015.

[44] S. M. Wheeler, L. A. Morrissey, S. N. Levine, G. P. Livingston, and W. F. Vincent, "Mapping cyanobacterial blooms in lake Champlain's Missisquoi bay using QuickBird and MERIS satellite data," *J. Great Lakes Res.*, vol. 38, pp. 68–75, 2012.

[45] K. H. Cheng, S. N. Chan, and J. H. W. Lee, "Remote sensing of coastal algal blooms using unmanned aerial vehicles (UAVs)," *Mar. Pollut. Bull.*, vol. 152, Mar. 2020, Art. no. 110889.

[46] Q. Zhu, J. Li, F. Zhang, and Q. Shen, "Distinguishing cyanobacterial bloom from floating leaf vegetation in Lake Taihu based on medium-resolution imaging spectrometer (MERIS) data," *IEEE J. Sel. Topics Appl. Earth Observ. Remote Sens.*, vol. 11, no. 1, pp. 34–44, Jan. 2018.

[47] D. Blondeau-Patissier, J. F. R. Gower, A. G. Dekker, S. R. Phinn, and V. E. Brando, "A review of ocean color remote sensing methods and statistical techniques for the detection, mapping and analysis of phytoplankton blooms in coastal and open oceans," *Prog. Oceanogr.*, vol. 123, pp. 123–144, Apr. 2014.

[48] Q. Liang, Y. Zhang, R. Ma, S. Loiselle, J. Li, and M. Hu, "A MODIS-based novel method to distinguish surface cyanobacterial scums and aquatic macrophytes in Lake Taihu," *Remote Sens.*, vol. 9, no. 2, Feb. 2017, Art. no. 133.

[49] B. Gokaraju, S. S. Durbha, R. L. King, and N. H. Younan, "Ensemble methodology using multistage learning for improved detection of harmful algal blooms," *Ieee Geosci. Remote Sens. Lett.*, vol. 9, no. 5, pp. 827–831, Sep. 2012.

[50] B. Gokaraju, S. S. Durbha, R. L. King, and N. H. Younan, "A machine learning based spatio-temporal data mining approach for detection of harmful algal blooms in the Gulf of Mexico," *IEEE J. Sel. Topics Appl. Earth Observ. Remote Sens.*, vol. 4, no. 3, pp. 710–720, Sep. 2011.

[51] C. Hu, "A novel ocean color index to detect floating algae in the global oceans," *Remote Sens. Environ.*, vol. 113, no. 10, pp. 2118–2129, Oct. 2009.

[52] Y. Oyama, T. Fukushima, B. Matsushita, H. Matsuzaki, K. Kamiya, and H. Kobinata, "Monitoring levels of cyanobacterial blooms using the visual cyanobacteria index (VCI) and floating algae index (FAI)," *Int. J. Appl. Earth Observ. Geoinf.*, vol. 38, pp. 335–348, Jun. 2015.

[53] P. Kowe, O. Mutanga, J. Odindi, and T. Dube, "Exploring the spatial patterns of vegetation fragmentation using local spatial autocorrelation indices," *J. Appl. Remote Sens.*, vol. 13, no. 2, Jun 10 2019, Art. no. 024523.

[54] W. Gong, S. Fang, G. Yang, and M. Ge, "Using a hidden Markov model for improving the spatial-temporal consistency of time series land cover classification," *ISPRS Int. J. Geo-Inf.*, vol. 6, no. 10, Oct 2017, Art. no. 292.

[55] Y. Zhang, K. Shi, Y. Zhou, X. Liu, and B. Qin, "Monitoring the river plume induced by heavy rainfall events in large, shallow, Lake Taihu using MODIS 250 m imagery," *Remote Sens. Environ.*, vol. 173, pp. 109–121, Feb 2016.

[56] S. N. Biswas, D. Rakshit, S. K. Sarkar, R. K. Sarangi, and K. K. Satpathy, "Impact of multispecies diatom bloom on plankton community structure in Sundarban mangrove wetland, India," *Marine Pollut. Bull.*, vol. 85, no. 1, pp. 306–311, Aug. 2014.

[57] J. Luo *et al.*, "Evaluating the influences of harvesting activity and eutrophication on loss of aquatic vegetations in Taihu Lake, China," *Int. J. Appl. Earth Observ. Geoinf.*, vol. 87, May. 2020, Art. no. 102038.

[58] T. Jia, X. Zhang, and R. Dong, "Long-term spatial and temporal monitoring of cyanobacteria blooms using MODIS on Google Earth Engine: A case study in Taihu Lake," *Remote Sens.*, vol. 11, no. 19, Oct. 2019, Art. no. 2269.

[59] S. Wang, W. Wang, J. Chen, B. Zhang, L. Zhao, and X. Jiang, "Characteristics of dissolved organic matter and its role in lake eutrophication at the early stage of algal blooms-a case study of Lake Taihu, China," *Water*, vol. 12, no. 8, Aug. 2020, Art. no. 2278.

[60] D. Xu and H. Chen, "Randomly directed and light winds exacerbate the emergence of large-scale cyanobacterial bloom area in Lake Taihu, China," *Appl. Ecol. Environ. Res.*, vol. 18, no. 3, pp. 4695–4708, 2020.

[61] C. Cheng, Y. Wei, G. Lv, and Z. Yuan, "Remote estimation of chlorophyll-a concentration in turbid water using a spectral index: a case study in Taihu Lake, China," *J. Appl. Remote Sens.*, vol. 7, no. 1, Dec. 2013, Art. no. 073465.

[62] C. Huang *et al.*, "Spatiotemporal variation in particulate organic carbon based on long-term MODIS observations in Taihu Lake, China," *Remote Sens.*, vol. 9, no. 6, Jun. 2017, Art. no. 624.

[63] W. Shi, Y. Zhang, and M. Wang, "Deriving total suspended matter concentration from the near-infrared-based inherent optical properties over turbid waters: A case study in Lake Taihu," *Remote Sens.*, vol. 10, no. 2, Feb. 2018, Art. no. 333.

[64] X. Yao *et al.*, "Emerging role of dissolved organic nitrogen in supporting algal bloom persistence in Lake Taihu, China: Emphasis on internal transformations," *Sci. Total Environ.*, vol. 736, Sep. 2020, Art. no. 139497.

[65] R. Ma, H. Duan, X. Gu, and S. Zhang, "Detecting aquatic vegetation changes in Taihu Lake, China using multi-temporal satellite imagery," *Sensors*, vol. 8, no. 6, pp. 3988–4005, Jun. 2008.

[66] J. Luo *et al.*, "A New method for modifying thresholds in the classification of tree models for mapping aquatic vegetation in Taihu Lake with satellite images," *Remote Sens.*, vol. 6, no. 8, pp. 7442–7462, Aug. 2014.

[67] D. Sun, Y. Li, Q. Wang, C. Le, C. Huang, and L. Wang, "Parameterization of water component absorption in an inland eutrophic lake and its seasonal variability: A case study in Lake Taihu," *Int. J. Remote Sens.*, vol. 30, no. 13, pp. 3549–3571, 2009, Art. no. 913310715.

[68] Z. Li, H. K. Zhang, D. P. Roy, L. Yan, H. Huang, and J. Li, "Landsat 15-m panchromatic-assisted downscaling (LPAD) of the 30-m reflectivewavelength bands to sentinel-2 20-m resolution," *Remote Sens.*, vol. 9, no. 7, Jul. 2017, Art. no. 755.

[69] D. Xu, D. Zhang, D. Shi, and Z. Luan, "Automatic extraction of open water using imagery of Landsat series," *Water*, vol. 12, no. 7, Jul. 2020, Art. no. 1928.

[70] K. Shi *et al.*, "Long-term MODIS observations of cyanobacterial dynamics in Lake Taihu: Responses to nutrient enrichment and meteorological factors," *Sci. Rep.*, vol. 7, no. 1, Jan. 2017, Art. no. 40326.

[71] C. Hu, Z. Lee, R. Ma, K. Yu, D. Li, and S. Shang, "Moderate resolution imaging spectroradiometer (MODIS) observations of cyanobacteria blooms in Taihu Lake, China," *J. Geophys. Res.-Oceans*, vol. 115, Apr. 2010, Art. no. C04002.

[72] A. A. Kurekin, P. I. Miller, and H. J. Van der Woerd, "Satellite discrimination of Karenia Mikimotoi and Phaeocystis harmful algal blooms in European coastal waters: merged classification of ocean colour data," *Harmful Algae*, vol. 31, no. 11, pp. 163–176, Jan. 2014.

[73] K. Shi *et al.*, "A semi-analytical approach for remote sensing of trophic state in inland waters: Bio-optical mechanism and application," *Remote Sens. Environ.*, vol. 232, Oct. 2019, Art. no. 111323.

[74] J. Li *et al.*, "Recovering low quality MODIS-terra data over highly turbid waters through noise reduction and regional vicarious calibration adjustment: A case study in Taihu Lake," *Remote Sens. Environ.*, vol. 197, pp. 72–84, Aug. 2017.

[75] C. Huang *et al.*, "Evaluation of the geostationary ocean color imager (GOCI) to monitor the dynamic characteristics of suspension sediment in Taihu Lake," *Int. J. Remote Sens.*, vol. 36, no. 15, pp. 3859–3874, 2015.

[76] R. R. Colditz, C. Troche Souza, B. Vazquez, A. J. Wickel, and R. Ressl, "Analysis of optimal thresholds for identification of open water using MODIS-derived spectral indices for two coastal wetland systems in Mexico," *Int. J. Appl. Earth Observ. Geoinf.*, vol. 70, pp. 13–24, Aug 2018.

[77] Z. Liu, Z. Yao, and R. Wang, "Assessing methods of identifying open water bodies using Landsat 8 OLI imagery," *Environ. Earth Sci.*, vol. 75, no. 10, May 2016, Art. no. 873.

[78] R. H. Becker *et al.*, "Unmanned aerial system based spectroradiometer for monitoring harmful algal blooms: A new paradigm in water quality monitoring," *J. Great Lakes Res.*, vol. 45, no. 3, pp. 444–453, Jun. 2019.

[79] M. Pinardi, A. Fenocchi, C. Giardino, S. Sibilla, M. Bartoli, and M. Bresciani, "Assessing potential algal blooms in a shallow fluvial lake by combining hydrodynamic modelling and remote-sensed images," *Water*, vol. 7, no. 5, pp. 1921–1942, May. 2015.

[80] K. Shi *et al.*, "Phenology of phytoplankton blooms in a trophic lake observed from long-term MODIS data," *Environ. Sci. Technol.*, vol. 53, no. 5, pp. 2324–2331, Mar. 2019.

[81] L. Wu *et al.*, "Discrimination of algal-bloom using spaceborne SAR observations of Great Lakes in China," *Remote Sens.*, vol. 10, no. 5, May 2018, Art. no. 767.

Dandan Xu received the B.S. and M.S. degrees in grassland remote sensing from Lanzhou University, Lanzhou, China, in 2011 and the Ph.D. degree in remote sensing from the University of Saskatchewan, Saskatoon, SK, Canada, in 2016.

She is currently an Associate Professor with the Department of Ecology, College of Biology and the Environment, Nanjing Forestry University, Nanjing, China. Her research interests include remote sensing and GIS application in ecosystems and environment.

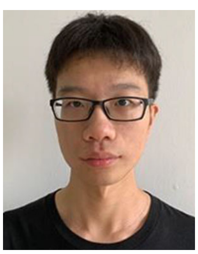

Yihan Pu received the B.S. degree in biological science from Jiangsu Normal University, Xuzhou, China, in 2019. He is currently working toward the M.S. degree in LiDAR and multispectral remote sensing application in evaluating canopy closure in forest plantations with the Department of Ecology, College of Biology and the Environment, Nanjing Forestry University, Nanjing, China.

His research interest includes ecological remote sensing.

Mengyuan Zhu received the B.S. degree in environment science from Nanjing Normal University, Nanjing, China, in 2009 and the Ph.D. degree in environment Science from the Nanjing Institute of Geography and Limnology, Chinese Academy of Sciences, Nanjing, China, in 2014.

She is currently an Assistant Professor with Nanjing Institute of Geography and Limnology, Chinese Academy of Sciences. Her research interests include dynamics of harmful algae, eutrophication mechanism, and nutrient dynamics in lake ecosystems.

Zhaoqing Luan received the B.S. degree in geography from Qufu Normal University, Qufu, China, in 1999, and the Ph.D. degree in environment science from Northeast Institute of Geography and Agroecology, Chinese Academy of Science, Changchun, China, in 2004.

He is currently a Professor with the Department of Ecology, College of Biology and the Environment, Nanjing Forestry University, Nanjing, China. His research interest includes in wetland ecology.

Kun Shi received the Ph.D. degree in remote sensing application from Nanjing Normal University, Nanjing, China, in 2013.

He is currently a Professor with Nanjing Institute of Geography and Limnology, Chinese Academy of Sciences, Nanjing, China, in the general field of water optics and remote sensing of aquatic ecosystems. His research interests include optical characteristics of inland water constituents, lake ecology, and the use of satellite data to trace the lake ecosystem responses to environmental change.